AIAA JOURNAL
Vol. 34, No. 3, March 1996

Demonstration and Characterization of Filtered Rayleigh Scattering for Planar Velocity Measurements

J. N. Forkey,* N. D. Finkelstein,* W. R. Lempert,† and R. B. Miles‡
Princeton University, Princeton, New Jersey 08544

Filtered Rayleigh scattering is an optical diagnostic technique that allows for simultaneous planar measurement of velocity, temperature, and pressure in unseeded flows. An overview of the major components of a filtered Rayleigh scattering system is presented. In particular, a detailed theoretical model is developed and discussed with associated model parameters and related uncertainties. Based on this model, results for two experimental conditions are presented: ambient room air and a Mach 2 freejet. These results include two-dimensional, spatially resolved measurements of velocity, temperature, and pressure derived from time-averaged spectra.

I. Introduction

FILTERED Rayleigh scattering (FRS), a recently developed flow diagnostic technique,[1,2] achieves large suppression of background scattering allowing planar flowfield visualization and obtains quantitative measurements of velocity, temperature, and density in unseeded gaseous flows. This technique makes use of Rayleigh scattering from molecules in the flow and is driven by a high-power, narrow linewidth, tunable, injection seeded laser. When imaging the scattered light onto a charge-coupled device (CCD) camera, unwanted background scattering from stationary objects may be filtered out by tuning the frequency of the narrow linewidth laser to coincide with an atomic or molecular absorption line and by placing a cell containing the atomic or molecular species between the camera and the flow. This cell acts as a notch filter, absorbing all background scatter at the laser frequency. Scattered light that is Doppler shifted, however, passes through the filter and is imaged on the camera.

Quantitative measure of flow properties is achieved by measuring the total intensity, Doppler shift, and spectral profile of the Rayleigh scattered light. The total intensity is directly proportional to density; the Doppler shift is directly proportional to velocity; and the spectral profile is a function of temperature and pressure. The scattering intensity, Doppler shift, and spectral profile are determined by passing the scattered light through the notch absorption filter and then by imaging it onto an intensified CCD camera. Because the filter absorbs light in a narrow frequency band, it converts the spectral information contained in the Doppler shift and Rayleigh profile into intensity information at the camera. By collecting data (camera pixel intensity) for varying conditions, v, T, and P may be determined.

Previous work has concentrated on the use of this technique for background suppression when visualizing flows and for the measurement of velocity. The background suppression feature of FRS has been used to image flowfields that otherwise would be completely obscured by the strong scattering from wind-tunnel surfaces. The authors have used this technique to image the flowfield inside a Mach 3 inlet and to generate volumetric images of the crossing shocks and boundary layer.[3] Elliott et al.[4] have also used this technique to observe structures in compressible mixing layers. The use of FRS to measure velocity was initially demonstrated using scattering from condensate particles in a Mach 2.5 airflow[5] and later in a Mach 5 unseeded nitrogen flow.[2] The measurement of velocity in a seeded compressible mixing layer was performed by Elliott et al.,[6] and velocities over a delta wing in a seeded airflow were measured by Meyers[7] using a technique similar to FRS called Doppler global velocimetry. This technique was also used by Smith and Northam[8] to image velocities in sonic and supersonic jets; limitations of the measurement capability of this technique have been investigated, theoretically, by McKenzie.[9] The use of FRS in unseeded flows for measuring mass flow has been investigated by Shirley and Winter.[10]

This article continues the development of FRS as a tool for measuring velocity in unseeded flows, by discussing the major sources of systematic uncertainties in FRS experiments and the techniques that have been developed to minimize them. The discussion begins with a theoretical model of the scattering and detection processes. This is followed by discussions of each of the three major components of an FRS experiment (laser, filter, and camera), along with corresponding analyses of the major sources of uncertainties. Experimental measurements are then presented along with a detailed error analysis of the planar velocity data obtained from an unseeded flow facility using a Nd:YAG laser together with a molecular iodine filter. Temperature and pressure data have also been measured. Although the error analysis for these parameters has not been performed with as much detail as for velocity, they are presented and discussed qualitatively. The article is concluded with a discussion of the development of ultraviolet FRS utilizing a frequency tripled Ti:sapphire laser and a mercury absorption filter. Although the discussions in this article focus on measurements made using molecular Rayleigh scattering, many of the considerations are directly applicable to experiments that make use of particle scattering.

II. Theoretical Model

For an FRS experiment, the pertinent raw data consist of grayscale value S, at a particular resolution element of the camera. When a laser pulse with energy per unit area of E_I, lineshape profile $l(\upsilon)$, and central laser frequency of υ_l, relative to some reference frequency, is incident on a region of flow with pressure P and temperature T, the Rayleigh scattered energy per unit frequency E_R at frequency υ relative to the reference frequency, scattered from an interrogation volume V into the solid angle $\mathrm{d}\Omega$, is given by

$$E_R(\lambda, \theta, \upsilon, P, T, \upsilon_l) = E_I \frac{PV}{kT} \frac{\mathrm{d}\sigma}{\mathrm{d}\Omega} \mathrm{d}\Omega \times \int_{-\infty}^{\infty} l(\upsilon - [\upsilon_l + \upsilon_D(\upsilon, \lambda, \theta)] - \upsilon') \times g(Y(P, T, \theta), \upsilon') \mathrm{d}\upsilon' \tag{1}$$

Here, the integral is a convolution between the laser lineshape $l(\upsilon)$ and the normalized Rayleigh–Brillouin scattering profile $g(Y, \upsilon)$; k is equal to Boltzmann's constant, and $\mathrm{d}\sigma/\mathrm{d}\Omega$ is the differential

Presented as Paper 95-0298 at the AIAA 33rd Aerospace Sciences Meeting, Reno, NV, Jan. 9–12, 1995; received Feb. 16, 1995; revision received Aug. 24, 1995; accepted for publication Sept. 18, 1995. Copyright © 1995 by the American Institute of Aeronautics and Astronautics, Inc. All rights reserved.

*Graduate Student, Department of Mechanical and Aerospace Engineering. Room D-414, Engineering Quad., Olden St. Student Member AIAA.

†Research Scientist, Department of Mechanical and Aerospace Engineering. Member AIAA.

‡Professor, Department of Mechanical and Aerospace Engineering. Senior Member AIAA.

Rayleigh scattering cross section. The laser lineshape $l(\upsilon)$ is centered at υ_l and the scattering is shifted by the Doppler shift υ_D (Ref. 11)

$$\upsilon_D = (2v/\lambda)\sin(\theta/2) \tag{2}$$

where v is the flow velocity in the direction that bisects the angle between the vector extending from the scattering center to the camera and the vector pointing opposite the laser propagation vector. Also, λ is the vacuum wavelength and θ the scattering angle. Here, the difference between the indices of refraction for air and vacuum has been neglected. The Rayleigh–Brillouin scattering profile $g(Y, \upsilon)$ is characterized by the Y parameter that is given by Tenti et al.[12] as

$$Y = \frac{nkT}{\sqrt{2}K v_0 \eta} \tag{3}$$

where n is the number density of the gas, η the viscosity, K the magnitude of the scattering wave vector,[11]

$$K = (4\pi/\lambda)\sin(\theta/2) \tag{4}$$

and v_0 the thermal velocity that is related to gas temperature and molecular mass m by[12]

$$v_0 = \sqrt{kT/m} \tag{5}$$

The Y parameter is a measure of the ratio of the scattering wavelength to the molecular mean free path.[12] This can be deduced from Eq. (3) by recognizing that viscosity η is linearly proportional to the product of molecular mass m, number density n, thermal velocity v_0, and mean free path. The Y parameter indicates the relative contribution of the central scattering peak and the two side peaks. A Y parameter much greater than 1 corresponds to strong side peaks, whereas a Y parameter much less than 1 corresponds to one central peak only. Substituting the given expressions for v_0 and K into Eq. (3), assuming the ideal gas law, and using the Sutherland formula for viscosity[13] yields an expression for Y in terms of flow parameters and scattering angle[14]

$$Y = 0.2308\left[\frac{T + 110.4}{T^2}\right]\left[\frac{P\lambda}{\sin(\theta/2)}\right] \tag{6}$$

Here, T has units of Kelvin, P has units of atmospheres, and λ has units of nanometers. Although a number of spectral models exist for $g(Y, \upsilon)$, the work reported here made use of the model developed by Tenti et al.[12] As discussed by Young and Kattawar,[15] it is generally agreed that the Tenti model most accurately represents Rayleigh–Brillouin scattering from air.

In addition to the Rayleigh signal, there is also some stray elastic scattering from stationary walls, windows, etc. This stray scattering has the same frequency and spectral profile as the laser,

$$E_E(\upsilon) = C_1 l(\upsilon - \upsilon_l) \tag{7}$$

where C_1 is a constant, proportional to the laser energy.

When the Rayleigh energy E_R and the stray scattering energy E_E are passed through the filter and imaged onto the camera, the final signal level S for one resolution element is given by

$$S = C_2\left[\int_{-\infty}^{\infty} E_R(\upsilon)t(\upsilon)\,\mathrm{d}\upsilon + \int_{-\infty}^{\infty} E_E(\upsilon)t(\upsilon)\,\mathrm{d}\upsilon\right] \tag{8}$$

where $t(\upsilon)$ is the transmission of the filter at frequency υ and C_2 a constant that takes into account transmission through the imaging system and conversion into grayscale data.

Equations (1–8) can be combined to show explicitly the parameters that influence S,

$$\begin{aligned} S(\lambda, \theta, R, B, v, P, T, \upsilon_l) &= R\frac{P}{kT}\int_{-\infty}^{\infty}\left\{\int_{-\infty}^{\infty} l(\upsilon - [\upsilon_l + \upsilon_D(v, \lambda, \theta)] - \upsilon') \right. \\ &\quad \left. \times\, g(Y(P, T, \theta), \upsilon')\,\mathrm{d}\upsilon'\right\} t(\upsilon)\,\mathrm{d}\upsilon \\ &\quad + B\int_{-\infty}^{\infty} l(\upsilon - \upsilon_l)t(\upsilon)\,\mathrm{d}\upsilon \end{aligned} \tag{9}$$

Here, R and B are the products of constants in Eqs. (1), (7), and (8), and may be considered calibration parameters. Also, λ is the absolute wavelength of the laser and is necessary only for calculating the Doppler shift and the Y parameter. Parameters v, P, and T are the unknowns in the experiment. Three independent unknowns require that at least three measurements of S be made while varying $t(\upsilon)$, θ, or υ_l. Varying $t(\upsilon)$ corresponds to simultaneous measurements of scattering through different absorption profiles (i.e., different cells). Varying θ corresponds to using either multiple laser angles or multiple viewing angles.[10] Varying υ_l corresponds to collecting signals at various different laser frequencies. Using multiple θ, or multiple cells with different $t(\upsilon)$, yields instantaneous information about flow parameters. For the work reported in this paper, however, time-averaged flow parameters were measured by tuning the laser. The main advantage of a time-averaged measurement was that shot noise was minimized so that systematic uncertainties could be investigated. Additionally, this enabled the accuracy of the theoretical spectral model to be evaluated.

The raw data obtained in such a frequency tuning experiment consisted of plots of resolution element signal S vs laser frequency υ_l. These plots were fit to Eq. (9) with v, T, and P taken as fitting parameters. For such a fit to yield accurate results, all fixed parameters in Eq. (9), that is, λ, θ, R, and B, had to be known or independently measured to some accuracy. The laser lineshape $l(\upsilon)$ and the filter cell absorption profile $t(\upsilon)$, also had to be known or independently measured. Any errors in these four parameters or two profiles propagated into systematic errors in the final values obtained for v, T, and P, according to the sensitivity analysis to be presented. Finally, the accuracy of the fit also depended on the accuracy with which the individual measurements of S and υ_l were made.

III. Measurement of Model Parameters

Each of the four parameters λ, θ, R, and B, the two profiles $l(\upsilon)$ and $t(\upsilon)$, and the two measurement quantities S and υ_l, along with uncertainties in each, is discussed in the following four subsections. In the first three subsections the major FRS subsystems are discussed. Uncertainties in everything but R and B were dictated by these subsystems. Values for R and B were found by calibration as discussed in the last subsection.

A. Filter

The filter consisted of a glass cell 2 in. in diameter and 4 in. long, with 2-in.-diam sleeves extending 2 in. beyond each of the two windows. A few iodine crystals were placed in the cell before it was evacuated and sealed. The temperature of the cell was measured and stabilized at 80°C by a temperature controller, a resistance temperature detector element cemented onto the cell wall, and heating tape, which covered the entire cell body and sleeves. The pressure of the cell was set by controlling the temperature of a side arm cold tip that was kept at a lower temperature than the cell body. The side arm was enclosed in a water jacket, and water temperature was set to 40°C by a water bath with a temperature accuracy of better than ±0.1°C.

To characterize the transmission profile of the filter, it was necessary to have a means of measuring the frequency of an interrogation laser relative to some absolute, stable reference. There was also a need to make similar measurements of the laser frequency υ_l while performing an actual FRS experiment. To this end, a heterodyne technique was used that measured frequency relative to the peak of the Doppler broadened iodine absorption line at 18789.0 cm^{-1}, that corresponds to the P142(37, 0) transition in the B-X electronic manifold.[16] The experimental apparatus used to characterize the absorption filter is shown in Fig. 1. The reference laser was a narrow linewidth (5 kHz), continuous wave (cw), 50-mW, Nd:YAG laser. A small portion of the fundamental infrared light at 1.064 μm was frequency doubled using a potassium titanyl phosphate (KTP) crystal. The 0.532-μm (green), frequency doubled light was separated from the fundamental, and passed through a 0.5-in.-diam iodine reference cell of construction similar to the filter cell with a main body temperature of 80°C and a sidearm temperature of 45.7°C. The light passed through this reference cell and was detected with an amplified photodiode. A standard first derivative nulling technique[17] was used to lock the frequency

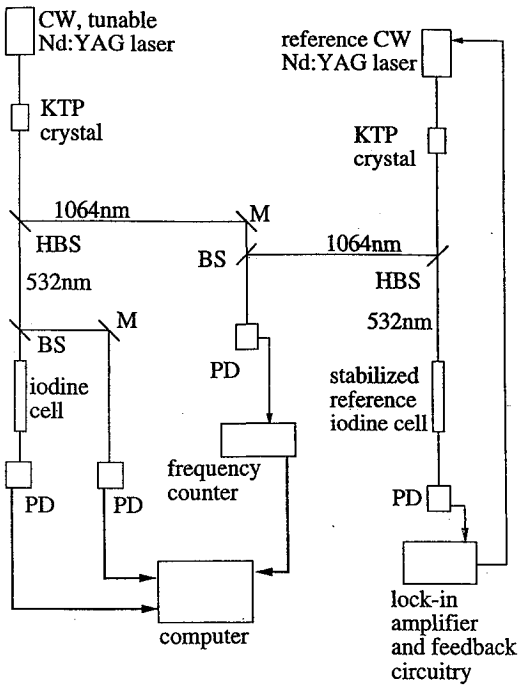

Fig. 1 Experimental apparatus used to characterize iodine cell; frequency reference apparatus on right, transmission measurement apparatus on left: BS, beamsplitter; HBS, harmonic beamsplitter; M, mirror; and PD, photodetector.

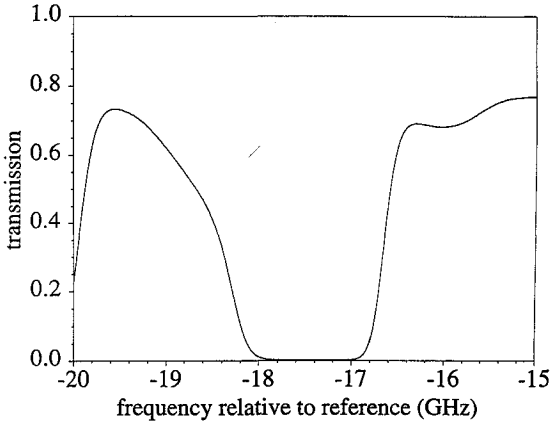

Fig. 2 Experimentally measured transmission profile of iodine filter cell, showing region used for experiments; 4-in.-long cell main body, 80°C main body temperature, and 40°C side arm temperature.

of the doubled beam of the reference laser to the P142(37, 0) absorption line. The residual infrared laser light from the reference laser was sent through a single mode, polarization preserving optical fiber onto a high-speed detector. A second, narrow linewidth, 40-mW, cw, Nd:YAG laser was used to determine the filter absorption spectrum by spectral tuning. The fundamental output of this laser was passed through a second KTP crystal to generate a second frequency doubled beam that was used to measure the filter transmission. The residual infrared light from this laser was passed through the same optical fiber onto the high-speed photodetector, where it interfered with the reference laser beam. The interference generated a heterodyne beat signal that corresponded to the frequency difference between the infrared beams and that was detected by a microwave frequency counter. This system allowed for frequency measurements (in the green) over a range of 80 GHz, with an estimated accuracy of ±2 MHz.

The measured transmission profile $t(\upsilon)$ is illustrated in Fig. 2. The maximum relative uncertainty in the transmission is estimated to be ±0.5%. Two additional transmission profiles were taken on two different days. During data analysis, each of the three transmission profiles, measured on three different days, were used independently resulting in negligible differences in the fitted values of v, T, and P.

B. Laser

The laser used was a commercial, injection seeded, frequency doubled, pulsed Nd:YAG laser. The absolute wavelength of the filter transition shown in Fig. 2, as measured by Gerstenkorn and Luc,[16] is 18788.4509 cm^{-1} (532 nm). During the FRS experiments, the frequency of the laser was tuned over approximately 5 GHz (0.17 cm^{-1}), which corresponds to a change in wavelength of 0.005 nm. This variation in wavelength resulted in negligible changes in the Doppler shift and Y parameter, and so both were calculated assuming λ to be 532 nm.

To determine the central frequency υ_l of the pulsed laser, a small portion of the infrared, cw seed laser was combined with the cw infrared beam from the reference laser already described. The same heterodyne system was then used to determine the frequency of the seed beam relative to the reference laser. Although the central frequency of the pulsed laser should be close to the measured value of the seed laser, it may differ slightly due to the Q-switch buildup time reduction technique used by the manufacturer to lock the pulsed laser to the seed laser. This technique requires that the oscillator cavity length be continuously dithered so that, even when the pulsed laser is well seeded, its frequency may still oscillate over a small range due to frequency pulling of the output pulse with respect to the seed frequency.[18] This frequency dither is specified by the manufacturer to be less than ±10 MHz at 532 nm. For the time-averaged FRS experiments to be reported on, the effect of this dither should be negligible, since, on average, half of the laser pulses will have a central frequency up to 10 MHz higher than the measured seed laser frequency, and half will have a central frequency up to 10 MHz lower. For instantaneous measurements, however, this frequency dither will introduce a nonnegligible (roughly 5 m/s) uncertainty in velocity.

Frequency tuning of the laser was accomplished by varying the seed laser temperature in discrete steps. It was found that this laser required roughly 10 s to stabilize after each step. Whereas this restabilization time dictated the speed with which data could be taken, the next generation of tunable lasers are expected to be tunable on a shot-to-shot basis, thereby decreasing the restabilization time by up to two orders of magnitude.

To characterize the laser frequency profile $l(\upsilon)$, a small portion of the pulsed laser beam was passed through the filter cell, and transmission was monitored as a function of laser frequency. The best fit to this data was obtained with a Gaussian laser line shape convolved with the measured transmission profile. Although this suggested that the use of a Gaussian line shape was appropriate, it did not rule out the possibility that some small Lorentzian component was also present. In any event, the linewidth of the Rayleigh–Brillouin scattering profile $g(Y, \upsilon)$ was much broader than the laser linewidth, and so a small discrepancy in the laser line shape should not have introduced a significant error in the measured flow parameters.

Although it is generally desirable to continuously monitor the laser pulse energy, in order to normalize data for any changes, it was determined that energy variations were small (less than 4%). Therefore, the laser pulse energy was not continuously monitored.

C. Camera

To test the linearity of the imaging system, a $\lambda/2$ plate and a linear polarizer were used to reduce the laser intensity in discrete steps. Camera response to the decreased intensity was determined by setting the camera and frame grabber parameters to the values used in the FRS experiments and monitoring the camera signal due to unfiltered Rayleigh scattering from air. Using this technique the camera was found to be linear to within ±2%.

The model already discussed assumes that the collection solid angle $d\Omega$, subtended by the camera lens, is small enough to consider $d\sigma/d\Omega$, υ_D, $g(Y, \upsilon)$, and $t(\upsilon)$ constants over the entire solid collection angle. To determine the conditions for which this assumption is valid, a computer model that does not make this assumption was developed, and its predictions compared to the simpler model.[19] For this theoretical study, an idealized Mach 5 flow, with velocity equal to 721 m/s, static temperature equal to 50 K, and static pressure equal to 40 torr was assumed. The laser sheet was assumed to have a propagation direction 45 deg relative to the flow, and the camera

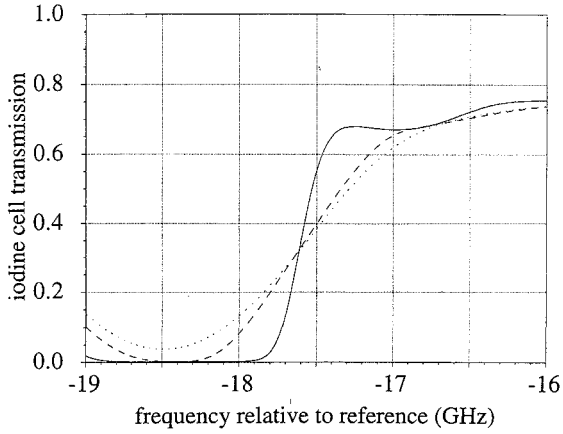

Fig. 3 Response of the iodine filter to scattering from an idealized Mach 5 flow, imaged with a collection f1. Assumed flow conditions were: velocity = 721 m/s, static temperature = 50 K, and static pressure = 40 torr; solid curve is the response predicted for narrow linewidth scattering when effects of the solid collection angle are neglected; dashed line includes the effects of the solid collection angle, again assuming narrow linewidth scattering; and dotted line includes the effects of the solid collection angle, as well as the Rayleigh–Brillouin scattering profile.

was assumed to image at an angle of 90 deg to the sheet. Filter transmission vs frequency plots were calculated for the point in the center of the field of view, using this more detailed model, assuming various collection f numbers and were compared to similar plots made using the simpler model described above. As can be seen in Fig. 3, a very small collection f number results in very different predictions from the two models, since the scattering angle θ varies significantly across the solid collection angle $d\Omega$, resulting in large variations in Doppler shift v_D and scattering profile $g(Y, v)$. As the collection f number increases, the variation of θ decreases, and so the discrepancy between the two models also decreases. For a collection f number greater than about 10, this discrepancy is small enough to be considered negligible.

For the experiments discussed below, the collection f number was approximately 15, so the variation in θ across the solid collection angle was neglected. It was still necessary, however, to accurately determine the value of θ referenced to the center of the collection lens. To do this, a HeNe laser at 632.8 nm was positioned so that it overlapped the ray extending from the center of the field of view to the center of the camera lens. By placing an index card in the HeNe beam at various locations, a spot was observed on the CCD. When the index card was in the object plane of the camera lens, the laser spot appeared as a small, focused spot; when the card was behind or in front of the object plane, the spot appeared as a much larger unfocused spot. The position and angle of the HeNe laser beam were varied until the in-focus spot and out-of-focus spot were both centered on the central pixel of the CCD chip. The scattering angle θ was then measured with a protractor. The accuracy of this measurement was limited by the accuracy with which the protractor could be read, and was estimated to be ± 1 deg. In larger facilities this same technique could be used to obtain much more accurate angle measurements since much longer lever arms could be used.

D. Parameters R and B

The two model parameters R and B indicate the relative contributions of the Rayleigh and background signals, respectively, to the total signal. R is given in units of grayscale multiplied by 10^{-20} cm^3, whereas B has units of grayscale. To determine these parameters, two intensity calibrations were performed, both with the filter cell removed from the front of the camera [i.e., $t(v) = 1$]. In the first calibration, the camera imaged an evacuated test section. With P equal to zero, Eq. (9) became $S = B$. For the second calibration, the camera imaged the test section at atmospheric conditions. In this case, P was assumed to be equal to 760 torr, and T was approximately 293 K (T was measured with a thermocouple for each calibration run). Equation (9) now became $S = (P/kT)R + B$, and since B was known from the first calibration, R was now determined. Typical values and uncertainties for R and B were 600 ± 20 and 40 ± 5, respectively.

IV. Measurements

A. Experimental Apparatus and Data Collection

Experiments were performed under two test conditions. The first condition consisted of ambient air at room temperature and pressure (nominally 0 m/s, 20°C, and 760 torr). Although the air was not moving, this test was a good indicator of the absolute velocity accuracy for the given temperature and pressure. The second test condition consisted of a Mach 2 freejet, pressure matched to ambient atmospheric pressure. The atmospheric air used for these experiments was compressed and dried by a commercial compressor and chemical dryer system. No condensation was observed in the Mach 2 jet.

The experimental apparatus is shown in Fig. 4. The laser beam was focused into a sheet and passed through the 6 × 6 in. vertical test section of a laboratory-scale wind tunnel. The scattering was captured orthogonal to the laser sheet, and the iodine cell was placed in front of the camera lens. The ambient air tests were performed with no flow in the wind tunnel, whereas the Mach 2 experiments utilized a pressure matched freejet roughly 6 mm in diameter, with a stagnation pressure of 100 psig, and a stagnation temperature of 258 K. Isentropic calculations predicted the streamwise velocity, static temperature, and static pressure at the exit of this jet to be 480 m/s, 143 K, and 753 torr, respectively. To achieve a significant Doppler shift, the Nd:YAG beam crossed the flow at an angle of 50.0 deg +/−0.5 deg. This required that the measurement region in the flow be some 12–22 mm (2–4 nozzle diameters) downstream of the nozzle exit in order to keep the laser beam from hitting the nozzle. RELIEF experiments[20] performed along a line 19 mm from the nozzle exit yielded velocities ranging from 477 to 497 m/s indicating that the flow in the FRS test region has interacted with the shear layers. Therefore, velocity, temperature, and pressure were not expected to be uniform, nor identical to the isentropically calculated values.

For each of the two test conditions, the R and B values were calibrated both before and after the collection of data. Additionally, during the calibration runs, a portion of the laser beam passed directly through the iodine absorption cell in order to determine a transmission vs frequency profile. This profile was used to correct for any long-term frequency drift of the reference laser frequency and to determine the laser linewidth as discussed earlier.

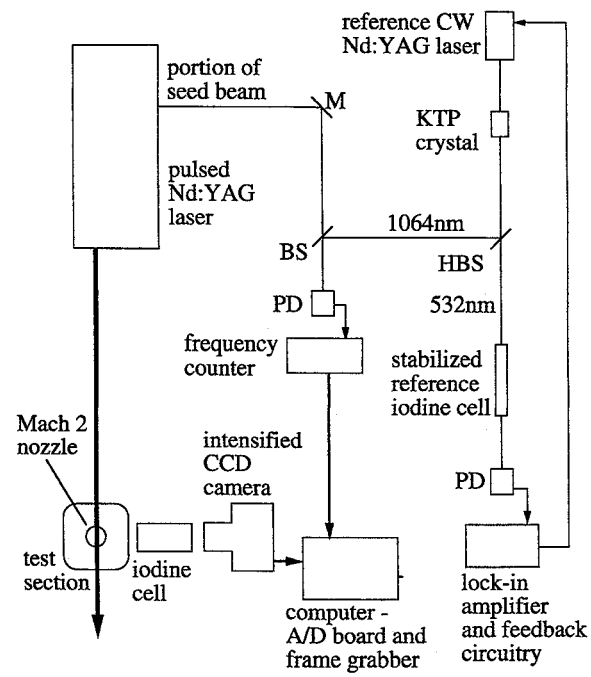

Fig. 4 Experimental apparatus for filtered Rayleigh scattering experiments; abbreviations as in Fig. 1.

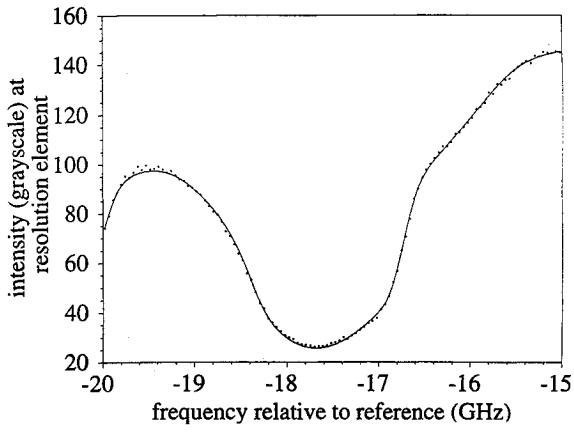

Fig. 5 Fit (solid line) of grayscale data values (points) to $S(\upsilon_l)$ as given by Eq. (9), for one resolution element from ambient air test case; nominal conditions: 0 m/s, 20°C, 760 torr.

A data run consisted of obtaining 50 frame averages at each of 110 different laser frequencies. These runs required approximately 50 min each for data collection; similar runs have since been performed with run times as short as 3 min. The image data were binned into 10×10 superpixels corresponding to approximately 300×300 μm spatial resolution of the object plane (each camera pixel had a linear physical dimension of roughly 20 μm). The choice of this resolution element size was influenced by previous work that indicated that the resolution of the microchannel plate was effectively 5×5 pixels on the CCD chip.[21] At each resolution element, an intensity vs frequency curve was generated and then fit to Eq. (9) using the Levenberg–Marquardt fitting procedure[22] with numerically calculated derivatives. Figure 5 shows the experimental data and the best least squares fit for a single, representative resolution element of the ambient air case. Similar fits, one at each resolution element, yielded values for v, T, and P at each point in the flow.

B. Uncertainty Analysis

To estimate the uncertainties in the final measurements of velocity, the uncertainties in the parameters θ, R, and B, and the uncertainty in the lineshape profile $l(\upsilon)$ were considered [uncertainty in λ, and $t(\upsilon)$ were negligible]. Although it is possible to independently calculate uncertainties for every point in the field of view, only a sample analysis of velocity uncertainty at a single point near the center of the field of view is presented here. The uncertainty in v is given by

$$\sigma_v^2 = \sum_{i=1}^{n} \left[\frac{\partial v}{\partial x_i} \right]^2 \sigma_{x_i}^2 \tag{10}$$

where x_i are the parameters in Eq. (9). The uncertainty in θ was estimated when it was measured. The uncertainties in R and B were estimated based on the variations between the pre- and postcalibration measurements at the various locations in the test region. The uncertainty in line shape $l(\upsilon)$ was presumed to be dominated by the uncertainty in the measured laser linewidth $\delta\upsilon$. Finally, the systematic uncertainty in υ_l arising due to uncertainty in the amount of long term drift of the reference frequency was accounted for by considering σ_{υ_r}, the uncertainty in the reference laser frequency. The uncertainties in linewidth $\delta\upsilon$ and the long-term drift of the reference frequency υ_r were estimated based on pre- and postcalibration values for a number of experiments. All of the partial derivatives used in Eq. (10), except $\partial v/\partial\theta$, were calculated numerically by fitting the data with the appropriate parameter changed slightly. The partial derivative $\partial v/\partial\theta$ was calculated analytically, by using Eq. (2). Table 1 shows the uncertainties in each of the parameters and profiles, the relevant partial derivatives for the first set of test conditions (ambient air), and the contribution to the total uncertainty from each of the parameters. The resulting total uncertainty in velocity was ±4 m/s. Table 2 shows the same data for the second test case (Mach 2 freejet), where the total uncertainty was ±5 m/s.

Table 1 Uncertainties for velocity measurement in ambient air

	θ, deg	R, cm^3 10^{-20}	B nondim.	$\delta\upsilon$, MHz	υ_r, MHz	Total uncertainty
typ. value	91	600	40	150	—	—
σ_{par}	1	20	5	50	5	—
$\partial v/\partial$(par)	0.011	0.008	0.25	0.002	0.65	—
σ_v, m/s	0.011	0.16	1.25	0.1	3.25	3.5

Table 2 Uncertainties for velocity measurement in Mach 2 jet

	θ, deg	R, cm^3 10^{-20}	B, nondim.	$\delta\upsilon$, MHz	υ_r, MHz	Total uncertainty
typ. value	91	600	40	150	—	—
σ_{par}	1	20	5	50	5	—
$\partial v/\partial$(par)	0.41	0.004	0.91	0.002	0.44	—
σ_v, m/s	0.41	0.08	4.55	0.1	2.2	5.1

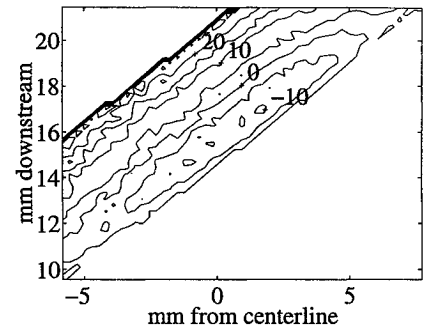

Fig. 6 Measured planar velocity profile of ambient air, in m/s; data are present only within the laser sheet, which extends from the top right to the bottom left. Note that the largest deviations from the expected value of 0 m/s occur near the edge of the laser beam.

C. Experimental Results

The planar velocity profile from the first test case, which has a uniform velocity of 0 m/s, is shown in Fig. 6. The laser sheet extends from the top right of the plot to the bottom left. Measured velocity values within the sheet range from −12 to 31 m/s; this indicates that the errors in these velocity measurements are considerably larger than those predicted in Table 1. As can be seen in Fig. 6, the errors are correlated with transverse location on the laser sheet. Two possible sources for these errors have been identified and are currently being investigated. The first is an observed change in the spatial mode of the laser sheet with laser frequency that results in a variation of local laser intensity with frequency. The functional form of these variations differs from point to point transversally across the sheet. Preliminary modeling of this effect has predicted velocity errors of the same sign and order of magnitude as those observed. The second source of error is a slight shift in the entire laser sheet, vertically, between the time of calibration and data collection. This may be due to heating of the turning mirrors, lenses, or optics in the beam path. Reducing the time between calibration and data scans should reduce or eliminate this problem. This error should be most apparent near the edge of the laser sheet where the gradient in R is largest. Neglecting this small portion of the laser sheet (where laser intensity is less than 75% of the peak intensity) yields a measured velocity range between −12 and 10 m/s.

Velocity values obtained with the Mach 2 freejet are shown in Fig. 7. The core of the jet exhibits velocities between 192 and 221 m/s for the velocity component measured, whereas the shear layers, apparent on either side of the core, exhibit velocities decreasing uniformly from 200 to 0 m/s. As in case 1, a significant variation is observed across the laser sheet, particularly in the low-energy region. However, for 100 independent points in a 10×10 point region in the center of the jet, and away from the edges of the laser sheet, the measured velocities were more uniform, with an average value of 205 m/s and a standard deviation of 5 m/s. The isentropic value for this velocity component is calculated to be 220 m/s, and Raman excitation plus laser induced electronic fluorescence (RELIEF) mea-

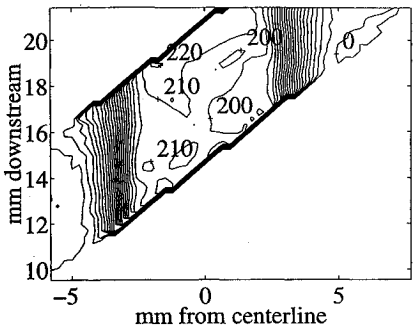

Fig. 7 Measured velocity values (in m/s) in the direction of FRS sensitivity, for Mach 2 jet. Although some of the variation observed in the core of the flow is due to laser sheet fluctuations, much of it is accounted for by jet structure measured independently with the RELIEF technique; expected velocity values based on isentropic calculation and RELIEF measurement are 220 m/s and 223 m/s, assuming flow direction is known precisely.

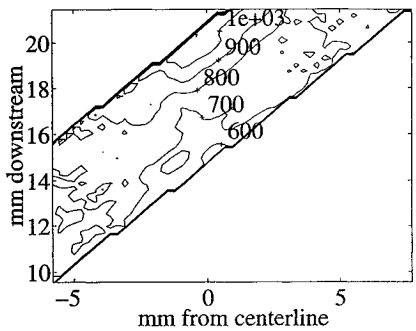

Fig. 8 Measured static pressure (torr) for the Mach 2 freejet; expected value for ideally pressure matched jet would be 760 torr.

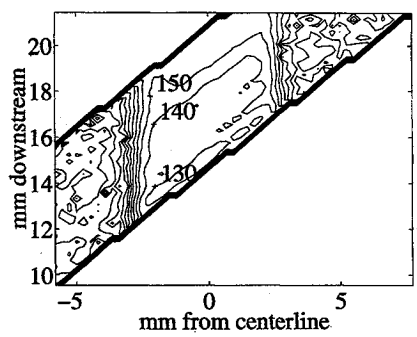

Fig. 9 Measured static temperature (K) for the Mach 2 freejet; core values agree well with the calculated isentropic value of 143 K.

surements yielded values ranging from 218 to 227 m/s across the core of the jet. It should be emphasized that the measured velocity was the velocity component along the direction of FRS sensitivity that was determined by the laser propagation direction and the camera observation direction. When comparing the measured core velocities to the isentropic and RELIEF values, these angles were measured relative to the exit surface of the nozzle and the jet was assumed to issue perpendicular to this surface. If the direction of the jet differed from the perpendicular by 1 deg, the isentropic and RELIEF values would change by 8 m/s.

Temperature and pressure data obtained from the FRS experiments for the Mach 2 conditions are presented in Figs. 8 and 9, respectively. Although the uncertainty analysis has not been performed in as much detail as for the velocity data, both temperature and pressure data show general behavior of the parameters as expected. The pressure of the freejet appears to be the same as that of the ambient surroundings, as expected from a pressure matched nozzle, although the pressure values vary across the entire region of interest. These variations are believed to be due in part to variations in the jet and in part to the transverse laser intensity variations already discussed. The temperature of the freejet is seen in Fig. 9 to be significantly lower than that of the ambient surroundings, as expected. Although the variation of measured temperature across the jet is ±17 K, the average value of 142 K agrees with the isentropically calculated value of 143 K.

V. Future Work

This work has emphasized the investigation of systematic uncertainties associated with FRS. Statistical uncertainties, however, due primarily to shot noise, must also be considered. Earlier discussions[19] for realistic conditions, using the Nd:YAG/iodine FRS configuration, and $f5$ optics, conclude that a CCD camera generates 64 photoelectrons per resolution element per laser pulse. This yields measured intensity variations of 1 part in 8, or 12.5%. Time averaging allows for the collection of a larger number of photons. By averaging 160 laser pulses, or 16 s at a 10-Hz repetition rate, at each measurement point, the shot noise is reduced to below 1%. However, this scheme prevents instantaneous measurements. Because the Rayleigh scattering cross section increases dramatically in the ultraviolet, due to the frequency υ^4 and index of refraction $(n-1)^2$ scaling, it is possible to collect in excess of 600 photoelectrons per laser pulse at 253.7 nm for the same experimental setup. The single pulse shot noise is reduced to an uncertainty of 2.4%.

The use of a frequency tripled, high-power, narrow linewidth, titanium:sapphire laser, in combination with a Hg filter, will therefore yield significant improvement. Current work is focused on developing such a laser system, in collaboration with Schwartz Electro-Optics, Inc.[23] To date, pulse energies in excess of 10 mJ of tunable, narrow linewidth, ultraviolet light have been achieved. The development of a mercury vapor filter for ultraviolet FRS is also under way. Because of the strong absorption and high atomic weight of mercury, very high optical depth is attainable. Model fits to experimental transmission scans of a 5-cm-long mercury vapor filter, suggest optical depths in excess of 1000 (Ref. 23). The high optical depth translates into an ability to suppress very strong unshifted stray scattering, while transmitting weaker Doppler shifted signals. Furthermore, the linewidth of the mercury absorption profile may be varied dramatically. This will lead to the tailoring of filters to experiments and to the use of multiple filters for instantaneous measurement of v, T, and P.

VI. Summary

The major components of a FRS experiment have been examined and sources of systematic uncertainties have been identified. Planar data was obtained in ambient air and in a Mach 2 jet with experimental uncertainties in velocity slightly larger than the predicted values of ±4 m/s and ±5 m/s. These were attributed to variations in the laser sheet spatial mode and to a slight shift in the laser sheet during experiments. Future work will continue the development of an ultraviolet FRS system that will reduce statistical uncertainty and make possible instantaneous measurements.

Acknowledgments

This work was conducted with the support of the U.S. Air Force Office of Scientific Research, NASA Langley and Lewis Research Centers, M. L. Energia, Inc., and Schwartz Electro-Optics, Inc. The authors would like to thank P. Howard for technical assistance, and G. Tenti, University of Waterloo, for making available to us his program for calculating Rayleigh–Brillouin profiles.

References

[1]Miles, R. B., and Lempert, W. R., "Two Dimensional Measurement of Density, Velocity, and Temperature, in Turbulent High Speed Air Flows by UV Rayleigh Scattering," *Applied Physics B*, Vol. 51, No. 1, 1990, pp. 1–7.

[2]Miles, R. B., Forkey, J. N., and Lempert, W. R., "Filtered Rayleigh Scattering Measurements in Supersonic/Hypersonic Facilities," AIAA Paper 92-3894, July 1992.

[3]Forkey, J. N., Lempert, W. R., Bogdonoff, S. M., Russell, G., and Miles, R. B., "Volumetric Imaging of Supersonic Boundary Layers Using Filtered Rayleigh Scattering Background Suppression," AIAA Paper 94-0491, Jan. 1994.

[4]Elliott, G. S., Samimy, M., and Arnette, S. A., "A Study of Compressible Mixing Layers Using Filtered Rayleigh Scattering," AIAA Paper 92-0175, Jan. 1992.

[5]Miles, R. B., Lempert, W. R., and Forkey, J., "Instantaneous Velocity Fields and Background Suppression by Filtered Rayleigh Scattering," AIAA Paper 91-0357, Jan. 1991.

[6]Elliott, G. S., Samimy, M., and Arnette, S. A., "Details of a Molecular Filter Based Velocimetry Technique," AIAA Paper 94-0490, Jan. 1994.

[7]Meyers, J. F., "Development of Doppler Global Velocimetry," AIAA Paper 94-2582, Jan. 1994.

[8]Smith, M. W., and Northam, G. B., "Application of Absorption Filter-Planar Doppler Velocimetry to Sonic and Supersonic Jets," AIAA Paper 95-0299, Jan. 1995.

[9]McKenzie, R. L., "Measurement Capabilities of Planar Doppler Velocimetry Using Pulsed Lasers," AIAA Paper 95-0297, Jan. 1995.

[10]Shirley, J. A., and Winter, M., "Air Mass Flux Measurement System Using Doppler Shifted Filtered Rayleigh Scattering," AIAA Paper 93-0513, Jan. 1993.

[11]Yeh, Y., and Cummins, H. Z., "Localized Fluid Flow Measurements with an He–Ne Laser Spectrometer," *Applied Physics Letters*, Vol. 4, No. 10, 1964, pp. 176–178.

[12]Tenti, G., Boley, C. D., and Desai, R. C., "On the Kinetic Model Description of Rayleigh–Brillouin Scattering from Molecular Gasses," *Canadian Journal of Physics*, Vol. 52, No. 4, 1974, pp. 285–290.

[13]White, F. M., "Preliminary Concepts," *Viscous Fluid Flow*, 2nd ed., McGraw–Hill, New York, 1991, pp. 27–29.

[14]Shimizu, H., Lee, S. A., and She, C. Y., "High Spectral Resolution Lidar System with Atomic Blocking Filters for Measuring Atmospheric Parameters," *Applied Optics*, Vol. 22, No. 9, 1983, pp. 1373–1381.

[15]Young, A. T., and Kattawar, G. W., "Rayleigh-Scattering Line Profiles," *Applied Optics*, Vol. 22, No. 23, 1983, pp. 3668–3670.

[16]Gerstenkorn, S., and Luc, P., *Atlas du Spectre d'Absorption de la Molecule Diode, Complement*, Pt. 8, Presses du CNRS, Lab. Aime Cotton, France, p. 34.

[17]Arie, A., Bortz, M. L., Fejer, M. M., and Byer, R. L., "Iodine Spectroscopy and Absolute Frequency Stabilization with the Second Harmonic of the 1319-nm Nd:YAG laser," *Optics Letters*, Vol. 18, No. 20, 1993, pp. 1757–1759.

[18]Park, Y. K., Guiliani, G., and Byer, R. L., "Unstable Single-Axial-Mode Operation of an Unstable Resonator Nd:YAG Oscillator by Injection Locking," *Optics Letters*, Vol. 5, No. 3, 1980, pp. 96–98.

[19]Miles, R. B., Forkey, J. N., Finkelstein, N. D., and Lempert, W. R., "Precision Whole-Field Velocity Measurements with Frequency Scanned Filtered Rayleigh Scattering," 7th International Symposium on Application of Laser Techniques to Fluid Mechanics, Paper 2-26, Lisbon, Portugal, July 1994.

[20]Miles, R. B., Connors, J., Markovitz, E., Howard, P., and Roth, G., "Instantaneous Supersonic Velocity Profiles in an Under Expanded Sonic Air Jet by Oxygen Flow Tagging," *Physics of Fluids A*, Vol. 1, No. 2, 1989, pp. 389–393.

[21]Kyritsis, D., private communication, Engine Lab., Mechanical and Aerospace Engineering Dept., Princeton Univ., Princeton, NJ, Nov. 1994.

[22]Bevington, P. R., "Least-Squares Fit to an Arbitrary Function," *Data Reduction and Error Analysis for the Physical Sciences*, 1st ed., McGraw–Hill, New York, 1969, pp. 204–246.

[23]Finkelstein, N. D., Gambogi, J., Lempert, W. R., Miles, R. B., Rines, G. A., Finch, A., and Schwarz, R. A., "Development of a Tunable Single Frequency Ultra Violet Laser Source for UV Filtered Rayleigh Scattering," AIAA Paper 94-0492, Jan. 1994.

AIAA Education Series

OPTIMIZATION OF OBSERVATION AND CONTROL PROCESSES

V.V. Malyshev, M.N. Krasilshikov, V.I. Karlov

1992, 400 pp, illus, Hardback, ISBN 1-56347-040-3, AIAA Members $49.95, Nonmembers $69.95, Order #: 40-3 (830)

This new book generalizes the classic theory of the regression experiment design in case of Kalman-type filtering in controllable dynamic systems. A new approach is proposed for optimization of the measurable parameters structure, of navigation mean modes, of the observability conditions, of inputs for system identification, etc. The developed techniques are applied for enhancing efficiency of spacecraft navigation and control.

About the Authors

V.V. Malyshev is Professor, Vice-Rector (Provost), Moscow Aviation Institute.

M.N. Krasilshikov is Professor at the Moscow Aviation Institute.

V.I. Karlov is Professor at the Moscow Aviation Institute.

Place your order today! Call 1-800/682-AIAA

AIAA

American Institute of Aeronautics and Astronautics

Publications Customer Service, 9 Jay Gould Ct., P.O. Box 753, Waldorf, MD 20604
FAX 301/843-0159 Phone 1-800/682-2422 8 a.m. - 5 p.m. Eastern

Sales Tax: CA residents, 8.25%; DC, 6%. For shipping and handling add $4.75 for 1-4 books (call for rates for higher quantities). Orders under $100.00 must be prepaid. Foreign orders must be prepaid and include a $20.00 postal surcharge. Please allow 4 weeks for delivery. Prices are subject to change without notice. Returns will be accepted within 30 days. Non-U.S. residents are responsible for payment of any taxes required by their government.